Modeling turbulence interaction with reacting iron particles

By S. Guhathakurta†, S. S. Hemamalini†, A. Ravi†, J. A. van Oijen†, B. Cuenot†, J. Wang, K. Maeda, H. Wang and X. C. Mi†

Iron powders have been proposed as a promising circular carrier of renewable energy. To develop practical energy-conversion technologies using iron-powder combustion, it is important to understand the complex interplay between the spatially discrete combustion of iron particles and turbulence. In this work, an Eulerian-Lagrangian simulation framework with point sources is developed to model burning iron particles in laminar and turbulent flows. To capture the effects of spatially discrete combustion, interparticle gradients in temperature, oxygen concentration and flow velocity are resolved with grid sizes significantly smaller than the mean particle spacing. In order to obtain numerically converged results, a distribution kernel method (DKM) is required to couple the Lagrangian sources to the gas-phase model. The capability of using a Gaussian DKM to achieve grid convergence for inert- and reactive-particle tests is demonstrated in this report. Sample results of a two-dimensional simulation showing the process of flame initiation in a stoichiometric ($\phi_{\mathrm{FeO}} = 1$) mixture of iron particle and air are provided.

1. Introduction

The abundance of renewable energy sources on our planet can potentially eliminate the use of fossil fuels, thus solving the energy and climate crisis currently faced by our society. What hinders us from transitioning to a carbon-neutral energy landscape is the fact that most of the major clean-energy sources are geographically scattered and highly intermittent. Therefore, a temporal and regional surplus of green power must be transformed into a transportable, storable and recyclable energy carrier. Iron powders have been proposed as a promising candidate for long-term storage and long-distance transport of clean energy owing to their carbon-free nature, high energy density and recyclability after combustion (Bergthorson 2018). To make the iron-based cycle of renewable energy, as illustrated in Figure 1, a reality, we need to design and optimize practical combustors of fine ($\propto$ 50–100μm) iron particles.

High-fidelity numerical simulations can be used to accelerate the design of iron-fuel combustors at reduced costs. As stabilized turbulent flames of iron particles lie at the heart of these practical combustors, it is important to understand the interplay between reacting iron particles and turbulence and to develop simulation tools that can accurately capture this complex interplay. Owing to a high boiling point, 3135 K, iron particles remain in condensed phases throughout the combustion process. As such, exothermic reactions take place at each particle and thus the spatial distribution of energy release is highly non-uniform on the scales of particle spacing. This unique feature arising from the combustion of nonvolatile fuel particles, referred to as spatially discrete combustion in the

† Department of Mechanical Engineering, Eindhoven University of Technology, The Netherlands

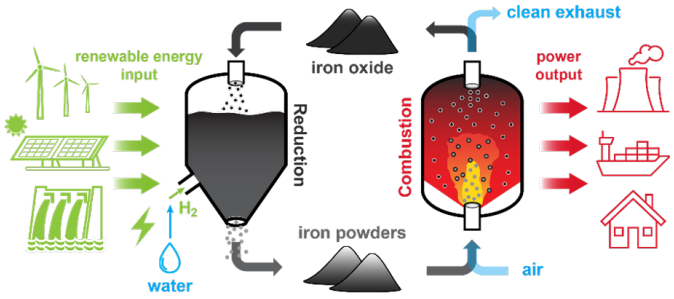

FIGURE 1. A carbon-free iron-based cycle of renewable energy.

literature (Goroshin *et al.* 2022), significantly differs from nearly continuous combustion of homogeneous gaseous mixtures, evaporating sprays or volatile solid fuels.

The ongoing efforts to model iron combustion are mainly focused on capturing the ignition and burning characteristics of isolated iron particles and laminar flames. This proposed study is the first attempt to elucidate the combustion of iron particles under turbulent flow conditions. To capture the spatially discrete nature of iron-particle combustion, it is essential to resolve the interparticle gradients in temperature, oxygen concentration and flow velocity. To achieve this resolution, a computational cell size that is at least one order of magnitude finer than the mean spacing of particles is required. Simulations with such fine resolutions are referred to as mesoscale-resolved simulations in this study. An Eulerian-Lagrangian modeling framework for mesoscale-resolved simulations of reacting point particles is reported here. These Lagrangian point sources are coupled with the Eulerian gas-phase model via distribution kernels.

This report is organized as follows. A dimensional analysis is provided in Section 2 elucidating the necessity of understanding the interplay between the spatially discrete combustion of iron particles and turbulent flows that arise in practical iron-powder combustors. Section 3 reports the detailed formulation for both gas-phase and particle models with different distribution-kernel approaches. The validation of particle model is provided in Section 4. Preliminary sample results of mesoscale-resolved simulations showing the process of flame initiation are reported and discussed in Section 5.

2. Dimensional analysis: why the interplay between turbulence and the reacting iron particle is important

Since heterogeneously reacting iron particles tend to induce interparticle gradients in gas-phase temperature, oxygen concentration and flow velocity, the mean particle spacing, l_p, is a key length scale anchoring the combustion dynamics of iron particles. The question thus arises as to how this l_p is compared to the characteristic length scales (i.e., the integral length scale, l and Kolmogorov length scale, l_k) of turbulent flows in practical iron-powder combustors.

The mean particle spacing l_p can be estimated knowing the initial mean particle size, $d_{\mathrm{p},0}$ and the initial concentration of iron mass, $C_{\mathrm{Fe},0}$. The initial concentrations of iron and oxygen injected into a combustor are related via the equivalence ratio. Although the overall stoichiometry of an iron-oxygen mixture is not uniquely defined due to multiple possible states of oxidation, an equivalence ratio considering FeO as the only product

can be defined as follows

$$\phi_{\mathrm{FeO}} = \frac{C_{\mathrm{Fe},0}/C_{\mathrm{O_2},0}}{2W_{Fe}/W_{O_2}}, \tag{2.1}$$

where W_{Fe} and $W_{\mathrm{O_2}}$ are the molar weights of iron and $\mathrm{O_2}$, respectively. For iron particles of $d_{\mathrm{p},0} = 50\mu$m, which is a typical size of iron powders used in practical combustors, mixed with air at standard conditions and $\phi_{\mathrm{FeO}} = 1$, the mean particle spacing is estimated to be $l_{\mathrm{p}} \approx 0.75\mu$m. The overall volume fraction of the particles is on the order of 10^{-4}.

To the authors' knowledge, laboratory-scale, swirl-stabilized turbulent combustors of iron powders have been independently developed at both McGill University and the Eindhoven University of Technology. Up to the time this report was written, neither the dimensions nor the operating parameters of these combustors had been published. For this high-level dimensional analysis, it is reasonable to assume that turbulent flow conditions created in these combustors are similar to those in laboratory-scale, swirl-stabilized coal combustors. Thus, the turbulent conditions of the Cambridge Coal combustor 1 (CCB1) (Balusamy *et al.* 2013) are considered in this analysis. In CCB1, the mixture of coal particles and air is injected from a tube of $d_{\mathrm{in}} = 15.8\mu$m at a mean velocity of 9.16 m/s. This injected flow corresponds to a Reynolds number of approximately 7500. Based on the experimental measurements and Taylor's hypothesis, the integral and Kolmogorov length scales are estimated to be $l = 6.08$mm and $l_{\mathrm{k}} = 0.11$mm, respectively (Balusamy *et al.* 2013).

Knowing the key length scales, the interaction between turbulence and particles can be characterized as follows:

(1) For particle volume fractions on the order of 10^{-4}, the two-way coupling between the particle and gas-phase dynamics is expected. For a particle volume fraction less than $0,4\%$, particle-particle interaction is negligible (Rizk & Elghobashi 1989).

(2) Typical particle sizes (e.g., 50μm) are comparable to or smaller than the Kolmogorov length scale, so that the viscous drag of the particles tends to dissipate the turbulent kinetic energy.

(3) Typical values of mean particle spacing are on the orders of 0.1–1mm, falling between the integral and Kolmogorov length scales of the turbulence. The spatially discrete energy release from the particles likely enhances the production of turbulent kinetic energy.

(4) For an integral length on the order of millimeters, given the large density of iron, the turbulent Stokes numbers of the particles are in the range of $Stk = 10$–100. The particles are poorly entrained by the flow.

Note that, in an industrial-scale combustor, e.g., a megawatt-level coal plant retrofitted by using iron powders, the length scales of turbulence are over one order of magnitude larger than those of laboratory-scale combustors, corresponding to a turbulent Stokes number that is one order of magnitude smaller for the same particle size. For both experimental and computational studies based on laboratory-scale combustors, prudence needs to be practiced in selecting the regimes of turbulent Stokes numbers that are representative of the conditions in large-scale combustors. Considering these characteristics of turbulent flows in a typical iron-powder combustor, simulations resolving the interparticle flow fields are required to gain insights into the multiscale interplay between reacting iron particles and turbulence.

3. Model description

3.1. *Particle model*

The particle modeling is similar to the work by Hazenberg & van Oijen (2021) with a reaction model following the framework proposed by Soo *et al.* (2022). As the flame temperature of iron in air ($\approx$ 2200K) is less than the boiling temperature of iron ($\approx$ 3100K) and iron oxides ($\approx$ 3400K), a heterogeneous combustion mode is considered in the current work. The position x_p and velocity u_p of the iron particles are tracked for each particle size,

$$\frac{dx_\mathrm{p}}{dt} = u_\mathrm{p}, \frac{du_\mathrm{p}}{dt} = \frac{3}{4}\frac{C_D\rho}{d_\mathrm{p}\rho_\mathrm{p}}|u-u_\mathrm{p}|(u-u_\mathrm{p}). \tag{3.1}$$

Drag forces are computed neglecting gravity,

$$\frac{\mathrm{d}u_\mathrm{p}}{\mathrm{d}t} = \frac{1}{\tau_\mathrm{p}}(u-u_\mathrm{p}), \tag{3.2}$$

with τ_p the relaxation time indicating how fast the particle adjusts its velocity to the gas velocity. Combining Eqs. (3.1) and (3.2) gives

$$\tau_\mathrm{p} = \frac{4}{3}\frac{\rho_\mathrm{p}d_\mathrm{p}}{\rho C_\mathrm{d}}\frac{1}{|u-u_\mathrm{p}|}. \tag{3.3}$$

The drag coefficient C_D is given by Schiller & Naumann (1933),

$$C_D = \frac{24}{Re}(1+0.15Re^{0.687}), \tag{3.4}$$

with Re the Reynolds number given by

$$Re = \frac{\rho|u-u_\mathrm{p}|d_\mathrm{p}}{\mu}, \tag{3.5}$$

in which d_p is the diameter of the particle, ρ is the density and μ is the dynamic viscosity of the gas. Subscript p indicates the properties of the particles, while no subscript is used for gas properties. For low Reynolds number (Stokes flow), the drag coefficient becomes $C_\mathrm{d} = 24/Re$ and the relaxation time becomes

$$\tau_\mathrm{p} = \frac{\rho_\mathrm{p}d_\mathrm{p}^2}{18\mu}. \tag{3.6}$$

The particle relaxation time was estimated to be on the order of the flame timescale, which indicates that drag and particle inertia effects are to be included in the modeling. For the chemical reactions, a single-step heterogeneous surface chemistry was assumed,

$$2\mathrm{Fe} + \mathrm{O}_2 \rightarrow 2\mathrm{FeO}. \tag{3.7}$$

The reaction rate of this surface reaction is modeled by an Arrhenius type equation,

$$k_r = k_0 \exp\left(\frac{-E_a}{R_u T_\mathrm{p}}\right), \tag{3.8}$$

where k_r is the surface reaction rate, k_0 is the pre-exponential factor, E_a is the activation energy, R_u is the universal gas constant and T_p is the particle temperature that is assumed to be uniform. Since this is a surface reaction, the oxygen has to diffuse to the surface of the particle from the surrounding gas. Depending on the conditions, the reaction rate can be limited by either surface kinetics or external diffusion of oxygen. A more physics-based

s	0.28	-	Mass-based stoichiometric ratio
ρ_{Fe}	7.874	g/cm^3	Iron density
ρ_{FeO}	5.745	g/cm^3	FeO density
C_{p}	0.677	J/(g K)	Specific thermal capacity of Fe and FeO
Δh_{c}	2906	J/g	Specific energy release
k_∞	75.0×10^7	cm/s	Pre-exponential factor
E_a/R_u	14.4×10^3	K	Activation temperature

TABLE 1. Parameters of the iron-particle model.

oxidation kinetic model that considers the hindering effect of a growing oxide layer (Mi *et al.* 2022) will be implemented in a future study. The overall mass consumption rate of iron is a combination of diffusion-limited and kinetic-limited regimes. The rate of change of mass of the particle m_{p} and the unreacted iron mass $m_{\mathrm{p,Fe}}$ can be calculated by

$$\frac{dm_{\mathrm{p}}}{dt} = \omega \cdot \pi d_{\mathrm{p}}^2, \quad \frac{dm_{\mathrm{p,Fe}}}{dt} = -\frac{1}{s}\frac{dm_{\mathrm{p}}}{dt}, \tag{3.9}$$

where s is the mass-based stoichiometric ratio. The convective heat transfer and enthalpy exchange due to the reaction of oxygen takes place according to

$$\frac{dH_{\mathrm{p}}}{dt} = k_{\mathrm{c}} A_{\mathrm{p}} (T_{\mathrm{p}} - T) + \frac{dm_{\mathrm{p}}}{dt} h_{\mathrm{O_2}}, \tag{3.10}$$

in which H_{p} is the enthalpy of the particle, k_{c} the convective heat transfer coefficient, T the temperature of the surrounding gas, T_{p} the particle temperature based on the particle enthalpy with effective heat capacity to account for the phase changes, $h_{\mathrm{O_2}}$ the enthalpy of oxygen and $k_{\mathrm{c}} = Nu\,\lambda_{\mathrm{f}}/d_{\mathrm{p}}$, λ_{f} the film layer thermal conductivity with Nu the Nusselt number (assumed constant $Nu = 2.0$). Table 1 contains various simulation parameters used in the model.

3.2. *Gas-phase model*

For the gas-phase modeling, nondimensional forms of continuity, momentum, energy and species mass conservation equations are used in NTMIX-CHEMKIN (developed at CERFACS) (Baum *et al.* 1994; Brouzet *et al.* 2021) as follows

$$\frac{\partial \rho}{\partial t} + \frac{\partial \rho u_j}{\partial x_j} = S_{\mathrm{M}}, \tag{3.11}$$

$$\frac{\partial \rho u_i}{\partial t} + \frac{\partial \rho u_i u_j}{\partial x_j} = -\frac{\partial p}{\partial x_i} + \frac{1}{Re_{ac}}\frac{\partial \tau_{ij}}{\partial x_j} + S_{\mathrm{F}}, \tag{3.12}$$

$$\frac{\partial \rho e_t}{\partial t} + \frac{\partial (\rho e_t + p) u_j}{\partial x_j} = \frac{1}{Re_{ac}}\frac{\rho(u_j \tau_{ij})}{\partial x_j} - \frac{1}{PrRe_{ac}}\frac{\partial q_j}{\partial x_j} + S_{\mathrm{H}}, \tag{3.13}$$

$$\frac{\partial \rho Y_\alpha}{\partial t} + \frac{\partial \rho Y_\alpha u_j}{\partial x_j} = -\frac{1}{Sc_\alpha Re_{ac}}\frac{\partial \rho Y_\alpha V_{\alpha j}}{\partial x_j} + W_\alpha \dot{\omega}_\alpha + S_{\mathrm{M},\alpha}, \tag{3.14}$$

where $Pr = \lambda_{\mathrm{ref}}/\mu_{\mathrm{ref}}$ is the reference Prandtl number and $Sc_\alpha = D_{\alpha,ref}/\mu_{\mathrm{ref}}$ is the reference Schmidt number of species α. The volumetric source terms accounting for the mass, momentum, heat and species mass transfer between gas and particles are denoted as S_{M}, S_{F}, S_{H} and $S_{\mathrm{M},\alpha}$, respectively. The nondimensional reaction rate is $\dot{\omega}_\alpha = \dot{\omega}_\alpha \rho_{\mathrm{ref}} c_{\mathrm{ref}}/L_{\mathrm{ref}}$. The acoustic Reynolds number is denoted as Re_{ac}.

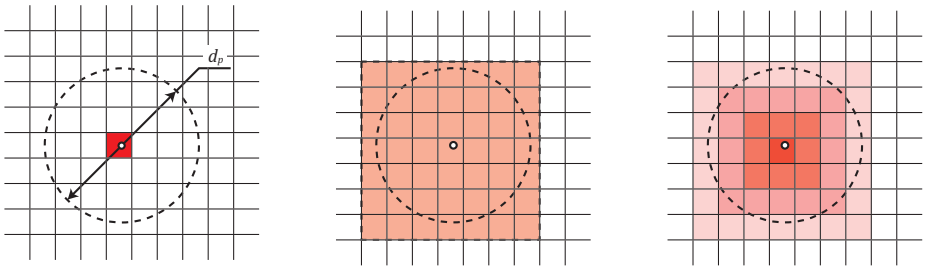

FIGURE 2. Types of particle-gas coupling: (left) particle-in-cell, (center) uniform distribution kernel, (right) Gaussian distribution kernel

3.3. *Coupling between the gas-phase and particle models: distribution-kernel methods*

In simulations where the particle size is smaller than the size of a mesh cell, interpolation methods can be used to transfer the Lagrangian source terms to the Eulerian mesh. However, to accurately model the spatially discrete combustion of iron particles, sufficient resolution equal to or smaller than the size of a particle is required. If the particle size is larger than the size of a mesh cell, the assumption that the particle is point-sourced is not optimal and coupling methods to sufficiently resolve the size of the particle are required.

In the present work, three coupling methods—particle-in-cell (PIC), uniform distribution kernel and Gaussian distribution kernel—are modelled to transfer the Lagrangian source terms to the Eulerian gas field. The latter two methods belong to a function group called distribution-kernel methods (DKMs). The PIC method transfers the Lagrangian source terms to a bounding box of Eulerian grid cells located nearest to the particle center. The PIC method is heavily dependent on the resolution of the mesh, and it is implemented and simulated to demonstrate the grid dependence of simple interpolation methods in cases where the particle size may be larger than the mesh resolution. The DKMs transfer the source terms to a number of mesh cells (the kernel) with a kernel size proportional to the particle diameter, thereby enveloping mesh cells fully or partially occupied by the particle. Such DKMs partially resolve the size of a particle by transferring the Lagrangian source terms to volumes scaling with the particle and not the mesh resolution. In the uniform DKM, the source terms are distributed equally to all the cells in the kernel, whereas in the Gaussian DKM, the source terms are distributed using a Gaussian function as follows

$$a_{(i,j,k)} = \frac{a}{\sigma_x \sigma_y \sigma_z (2\pi)^{3/2}} \exp\left\{-\frac{1}{2}\left[\left(\frac{x_i - x_\mathrm{p}}{\sigma_x}\right)^2 + \left(\frac{y_i - y_\mathrm{p}}{\sigma_y}\right)^2 + \left(\frac{z_i - z_\mathrm{p}}{\sigma_z}\right)^2\right]\right\}, \tag{3.15}$$

where a is an arbitrary source term, (i, j, k) is an arbitrary cell in the kernel, (x_i, y_i, z_i) is the location of the kernel cell center, $(x_\mathrm{p}, y_\mathrm{p}, z_\mathrm{p})$ is the location of the particle center and σ_x, σ_y and σ_z the standard deviations of the Gaussian function in x-, y- and z- axes, respectively. In the case of a 2D simulation, a similar 2D Gaussian function is employed. A figurative representation of the three coupling methods is presented in Figure 2.

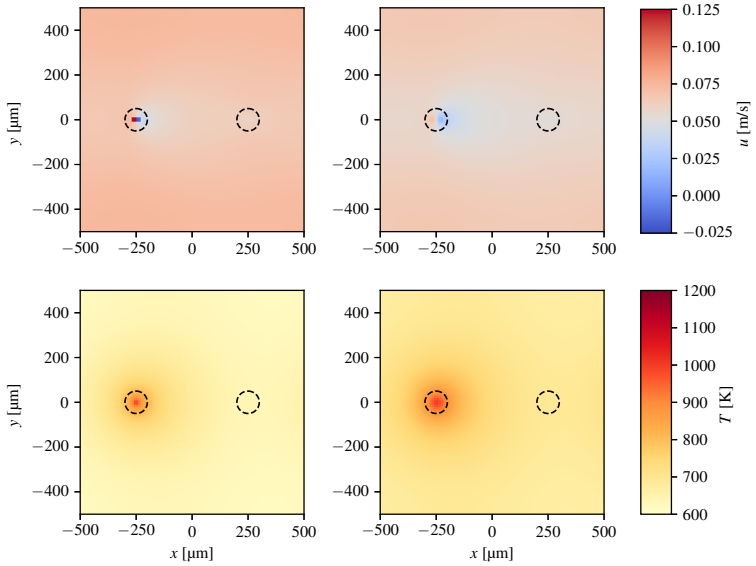

FIGURE 3. Contours of the x-component of gas velocity at flow time $t = 20$ms at mesh a resolution of 10μm: (left) particle-in-cell and (right) Gaussian distribution-kernel method.

4. Implementation of the particle model and evaluation of distribution kernel methods

The particle model and the coupling methods are first compared through two-dimensional flow (with inert particles). The simulations with inert particles in mean flow are used to analyze the consequences of the coupling methods on modeling the drag and thermal effects exerted by the particles on a flow. In the present work, the effects of mesh resolution are tested for two coupling methods—particle-in-cell (PIC) and the Gaussian distribution kernel (DKM). The domain, of size 1mm in x-, y- and z-directions, is initialized with air at a mean flow of $u = 10$cm/s in the x-direction and at a pressure and temperature of 1 atm and 300 K, respectively. Periodic boundary conditions are used throughout the domain. Two fixed inert particles of diameters $d_\mathrm{p} = 50\mu$m are initialized at temperatures 1000 K and 300 K and placed at 0.25 mm from the $-x$ and $+x$ boundaries, respectively. The simulations are carried out for mesh resolutions of 10μm and 20μm to a maximum flow time of 20 ms.

Figure 3 presents a visual comparison of x-component of gas velocity u_x and gas temperature T_p at the same flow time, at a mesh resolution of 10μm, which is one-fifth of the particle diameter. From Figure 3, it is observed that the PIC coupling method results in values of very high magnitude of u_x at the location of the particle center and consequently results in steep gradients. This is further affirmed from Figure 4. The PIC coupling also exhibits a difference in the values of u_x and T, with different mesh resolutions, inferring grid dependence. The values of u_x and T as simulated using a Gaussian DKM show grid independence. Furthermore, the velocity profile using a Gaussian DKM portray gradients spanning a distance approximating the particle size. The Gaussian DKM also results in higher heat dissipation than the PIC method, as seen in Figures 3 and 4. This is expected, since the Gaussian DKM method distributes heat at mesh locations away from the particle center within a single timestep, whereas, in the case of the PIC method,

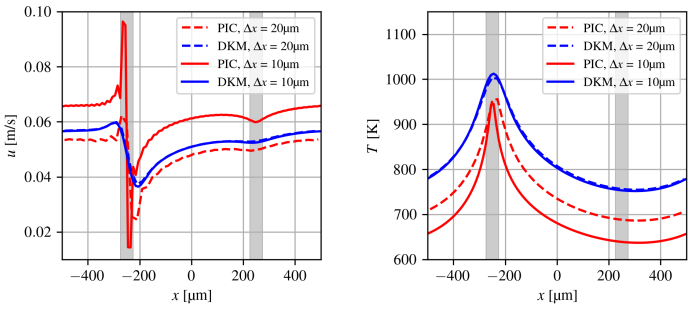

FIGURE 4. (Left) The $x-$component of gas velocity u_x and (right) the gas temperature T in center of domain along the flow direction for particle-in-cell (PIC) and Gaussian DKM coupling methods at $t = 20$ ms for different mesh resolutions; particle locations are indicated in gray.

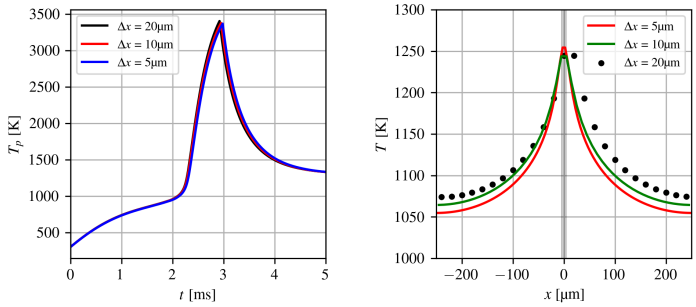

FIGURE 5. (Left) Time evolution of the temperature of a reacting particle at various mesh resolutions. (Right) Comparison of gas temperature in the center of the domain along the x-direction at $t = 2.859$ ms for different mesh resolutions.

additional time steps are required to dissipate source quantities from the particle center to the circumference of the particle.

Two-dimensional simulations of combustion are carried out with a different case setup that ensures ignition of the particle. Hence, a domain size of 0.5 mm in all directions with periodic boundaries throughout the domain is used for simulations of combustion. The domain is initialized with air at a pressure of 1 atm and a temperature of 1000 K with no background flow. A single reactive iron particle of diameter $d_\mathrm{p} = 10\mu$m and temperature $T_\mathrm{p} = 300$ K is fixed at the center of the domain. The Gaussian DKM is tested at mesh resolutions of 5μm and 10μm, and the results are compared to the PIC coupling at a mesh resolution of 20μm. The time evolution of the particle temperature, shown in Figure 5, shows good agreement between the three different mesh resolutions. The gas temperature in the radial direction from the particle center shows minimal differences with the different mesh resolutions.

5. Results and discussion

Sample results of a two-dimensional simulation showing the initiation process of a flame in a stoichiometric (i.e., $\phi_\mathrm{FeO} = 1$) suspension of iron particles with an initial size of $d_{\mathrm{p},0} = 10\mu$m in air at $T_{\mathrm{g},0} = 300$K and $p_0 = 1$ atm are provided in Figure 6. The mean particle spacing is $l_\mathrm{p} = 150\mu$m. The simulation is performed in a 1mm $\times$ 1mm

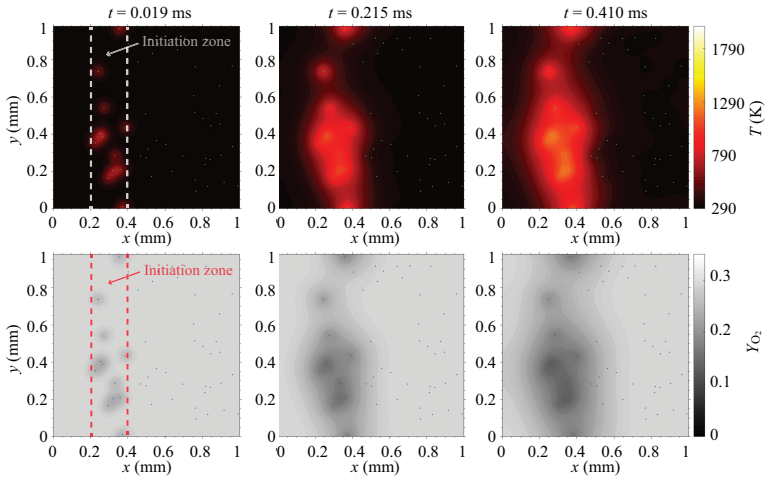

FIGURE 6. Sample results of a two-dimensional simulation showing the process of flame initiation for a case with iron particles of $d_{p,0} = 10\mu$m and $\phi_{FeO} = 1$: upper row—gas temperature, lower row—oxygen mass fraction.

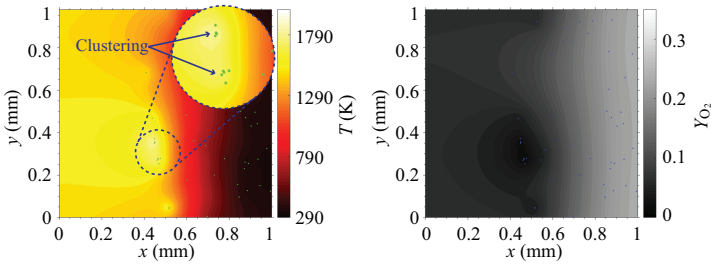

FIGURE 7. Sample results of a two-dimensional simulation showing the process of flame initiation for the same case as shown in Figure 6 at a later time when a flame front is established. The inset shows the clustering of particles.

square domain and the one-cell depth in the z-direction is selected to be l_p so that the mass of gaseous oxygen in the domain is consistent with the designated equivalence ratio. The upper and lower rows in Figure 6 show the fields of gas temperature and oxygen mass fraction, respectively. The vertical dashed lines indicate an initiation zone wherein the particles are initially at 1200 K. The left boundary of the domain is an open end, i.e., with an outlet boundary condition and the right boundary is a closed end. The hot particles in the initiation zone transfer heat and consume oxygen from the surrounding gas. The resulting heat wave propagates rightward to ignite the initially cold particles. The interparticle gradients in temperature and oxygen concentration are resolved by simulation.

Figure 7 shows the temperature and Y_{O_2} fields at a later time when a flame front is established. Behind the flame front, the spatial distributions of temperature and Y_{O_2} are relatively uniform. This resulting flame structure is due to the fact that the energy release time (or the characteristic scale of reaction time) is significantly greater than the timescale of interparticle heat and mass transport. A more nonuniform flame structure likely arises in cases with fuel-lean mixtures or larger particles, wherein the mean particle spacing is greater so that the interparticle diffusion timescale is longer. As indicated in

Figure 7, a tendency toward clustering is observed in a region where the gas is heated more rapidly due to several more closely located hot particles. The detailed mechanism underlying this clustering phenomenon will be investigated in future work.

6. Concluding remarks

The interaction between reacting iron particles and turbulence in practical combustors is demonstrated to be of importance via a dimensional analysis comparing the key length scales of the turbulence (i.e., the integral and Kolmogorov lengths) and particles (i.e., particle sizes and the mean spacing). Mesoscale-resolved simulations can provide insights into the interplay between the spatially discrete combustion of iron particles and turbulent flows. This report documents the model development for achieving such simulation capabilities. The preliminary tests show that Eulerian-Lagrangian simulation with point sources and Gaussian distribution kernels (to couple the gas-phase and particle models) is a promising approach to obtain numerically converged results for flows with reacting iron particles. The distribution-kernel methods can be further improved using data from particle-resolved direct numerical simulations.

Acknowledgments

The authors thank Magnus Vartdal (Norwegian Defence Research Establishment) and Sourabh Apte (Oregon State University) for the fruitful discussion on how to improve the distribution kernel method for point sources during the CTR Summer Program.

REFERENCES

Balusamy, S., Schmidt, A. & Hochgreb, S., 2013 Flow field measurements of pulverized coal combustion using optical diagnostic techniques. *Exp. Fluids* **54**, 1–14.

Baum, M., Poinsot, T. J., Haworth, D. C., & Darabiha, N. 1994 Direct numerical simulation of $H_2/O_2/N_2$ flames with complex chemistry in two-dimensional turbulent flows. *J. Fluid Mech.* **281**, 1–32.

Bergthorson, J. M. 2018 Recyclable metal fuels for clean and compact zero-carbon power. *Prog. Energy Combust. Sci.* **68**, 169–196.

Brouzet, D., Talei, M., Brear, M. J., & Cuenot, B. 2021 The impact of chemical modeling on turbulent premixed flame acoustics. *J. Fluid Mech.* **915**, A3.

Goroshin, S., Palecka, J. & Bergthorson, J. M. 2022 Some fundamental aspects of laminar flames in nonvolatile solid fuel suspensions. *Prog. Energy Combust. Sci.* **91**, 100994.

Hazenberg, T. & van Oijen, J. A. 2021 Structures and burning velocities of flames in iron aerosols. *Proc. Combust. Inst.* **38**, 4383–4390.

Soo, M., Mi, X., Goroshin, S., Higgins, A. J., & Bergthorson, J. M. 2018 Combustion of particles, agglomerates, and suspensionsA basic thermophysical analysis. *Combust. Flame* **192**, 384–400.

Mi, X. C., Fujinawa, A. & Bergthorson, J. M. 2022 A quantitative analysis of the ignition characteristics of fine iron particles. *Combust. Flame* **240**, 112011.

Rizk, M. A. & Elghobashi, S. E. 1989 A two-equation turbulence model for dispersed dilute confined two-phase flows. *Int. J. Multiph. Flow* **15**, 119–133.

Schiller, L. & Naumann, A. Z. 1933 Über die grundlegenden Berechnungen bei der Schwerkraftaufbereiting. *Z. Ver. Deut. Ing.* **77**, 318-321.